Molecular Vision 2015; 21:244-263 <http://www.molvis.org/molvis/v21/244>
Received 14 November 2014 | Accepted 5 March 2015 | Published 7 March 2015

Activation and quenching of the phototransduction cascade in retinal cones as inferred from electrophysiology and mathematical modeling

Luba Astakhova, Michael Firsov, Victor Govardovskii

Institute for Evolutionary Physiology and Biochemistry, Russian Academy of Sciences

Purpose: To experimentally identify and quantify factors responsible for the lower sensitivity of retinal cones compared to rods.

Methods: Electrical responses of frog rods and fish (*Carassius*) cones to short flashes of light were recorded using the suction pipette technique. A fast solution changer was used to apply a solution that fixed intracellular Ca^{2+} concentration at the prestimulus level, thereby disabling Ca^{2+} feedback, to the outer segment (OS). The results were analyzed with a specially designed mathematical model of phototransduction. The model included all basic processes of activation and quenching of the phototransduction cascade but omitted unnecessary mechanistic details of each step.

Results: Judging from the response versus intensity curves, *Carassius* cones were two to three orders of magnitude less sensitive than frog rods. There was a large scatter in sensitivity among individual cones, with red-sensitive cones being on average approximately two times less sensitive than green-sensitive ones. The scatter was mostly due to different signal amplification, since the kinetic parameters of the responses among cones were far less variable than sensitivity. We argue that the generally accepted definition of the biochemical amplification in phototransduction cannot be used for comparing amplification in rods and cones, since it depends on an irrelevant factor, that is, the cell's volume. We also show that the routinely used simplified parabolic curve fitting to an initial phase of the response leads to a few-fold underestimate of the amplification. We suggest a new definition of the amplification that only includes molecular parameters of the cascade activation, and show how it can be derived from experimental data. We found that the mathematical model with unrestrained parameters can yield an excellent fit to experimental responses. However, the fits with wildly different sets of parameters can be virtually indistinguishable, and therefore cannot provide meaningful data on underlying mechanisms. Based on results of Ca^{2+}-clamp experiments, we developed an approach to strongly constrain the values of many key parameters that set the time course and sensitivity of the photoresponse (such as the dark turnover rate of cGMP, rates of turnoffs of the photoactivated visual pigment and phosphodiesterase, and kinetics of Ca^{2+} feedback). We show that applying these constraints to our mathematical model enables accurate determination of the biochemical amplification in phototransduction. It appeared that, contrary to many suggestions, maximum biochemical amplification derived for "best" *Carassius* cones was as high as in frog rods. On the other hand, all turnoff and recovery reactions in cones proceeded approximately 10 times faster than in rods.

Conclusions: The main cause of the differing sensitivity of rods and cones is cones' ability to terminate their photoresponse faster.

Vision in vertebrates covers an enormous range of natural illumination levels that spans over 11 orders of magnitude. This unique ability is supported by the presence of two kinds of photoreceptor cells in the retina, namely rods and cones. Rods are photoreceptors of nocturnal vision. They are highly sensitive and can reliably signal arrivals of single photons. High sensitivity, however, makes rods susceptible to saturation; thus, for example, human rod monochromats (persons whose retina lacks functional cones) are light-blinded even at low diurnal levels of illumination [1]. Diurnal photoreceptors, cones, are 100- to 1,000-fold less sensitive than rods. Cones do not saturate and provide useful vision at the maximum intensities available in nature.

The biochemical and physiological mechanisms that ensure high sensitivity of rods are fairly well understood. The rod visual pigment, rhodopsin (R), belongs to the family of G-protein coupled receptors (GPCRs). Upon absorption of light, rhodopsin efficiently interacts with its cognate trimeric GTP-binding protein, transducin (T), and produces its active form, T* (T_α-GTP). Due to the enzymatic nature of the reaction, a single photoactivated rhodopsin (R*) produces hundreds of T*s per second. Each T* activates a catalytic subunit of the effector enzyme cGMP-phosphodiesterase (PDE). This greatly increases the rate of hydrolysis of the cytoplasmic secondary messenger, cGMP. The concentration of cGMP drops, which leads to the closure of the cGMP-gated

Correspondence to: Victor Govardovskii, IEPHB RAS, 44 Thorez prospect, 194223 St. Petersburg, Russia; Phone: (7)-(812)-5504989; FAX: (7)-(812)-5504989; email: vgovardovski@yahoo.com

ionic channels (cyclic nucleotide-gated [CNG] channels) in the plasma membrane of the outer segment (OS), thereby generating the electrical response.

The light-activated cascade is quenched by mechanisms operating at each activation step. The activity of R* is decreased by multiple phosphorylation by rhodopsin kinase and finally blocked by binding of arrestin. The active T_{α}GTP-PDE* is turned off by its intrinsic GTPase activity, which is enhanced by the interaction with the GTPase activating complex, RGS-9/Gβ5. Hydrolyzed cGMP is replenished by continuously running guanylate cyclase (GC), which returns the rod to its prestimulus state. Recovery of the dark state is greatly enhanced by negative feedback regulations that are controlled by the cytoplasmic concentration of Ca^{2+} ions. Ca^{2+} enters the OS via the CNG channels and is pumped out by the Na^{+}/Ca^{2+}-K^{+} exchanger (NCKX). Light closure of the CNG channels reduces the Ca^{2+} influx, thereby causing a decrease in $[Ca^{2+}]_{in}$. This decrease accelerates the phosphorylation (hence turnoff) of R* by rhodopsin kinase via the Ca^{2+}-sensing protein recoverin, and increases the production of cGMP by GC via GC-activating proteins (GCAPs). In addition, the decrease of $[Ca^{2+}]_{in}$ increases the affinity of the CNG channels to cGMP so that they stay open at lower cGMP concentration. Ca^{2+} feedback contributes greatly to shaping photoresponses and plays an important role in light adaptation, the process that prevents the saturation of photoreceptors by steady illumination.

The mechanisms of rod excitation and light adaptation have been studied in unprecedented detail using biochemical, molecular, electrophysiological, and genetic methods, and extensively reviewed (since 2000, see [2-17]). This, however, cannot be said about cones. It is generally believed that the basic principles of cone functioning are similar to those of rods. Nevertheless, the mechanisms by which cones reduce their sensitivity by 100- to 1,000-fold and avoid saturation at maximum possible illuminance levels are poorly understood. Most proteins of the phototransduction cascade exist in a rod- or cone-specific version, and could account for the observed differences between the two types of photoreceptors. Basically, the photoreceptor sensitivity is set by a balance between two factors, the rate of the light-induced activation of the cGMP hydrolysis, and the speed of its turnoff. The latter certainly plays the leading role, as is seen from the fact that the photoresponses in cones are an order of magnitude briefer compared to rods. The role of the former factor, which could be called biochemical amplification, is still controversial.

Biochemical amplification is the product of the speed of generation of T* by a single R* and the speed of the cGMP hydrolysis by PDE*. Thus, the amplification in cones can be reduced either by less efficient interaction of cone visual pigments with cone transducin, lower catalytic activity of cone PDE, or both. As for the catalytic properties of cone PDE, they are probably not much different from those of rod PDE. The maximum hydrolysis rate per PDE subunit of the two enzymes is the same, from 2,000 to 2,700 s^{-1} (frog rods [18], bovine cones [19], chipmunk cone-dominant preparation [20], bovine rod and cone PDE subunits expressed and tested in various combinations [21,22]). Michaelis' constant of cone PDE may be a bit higher than that of rod PDE (17 to 26 μM in cones [19,22,23] versus 10 to 17 μM in rods [18,23]).

As for the activation of transducin/PDE by a cone visual pigment, the most direct biochemical assays in vitro show that it is apparently two- to fivefold slower than the activation by rhodopsin. This was shown for chicken [24,25], human [26], and mouse green cone pigments [25]. Kawamura's group [27-29] used the most intact preparations of carp rod and cone photoreceptor membranes. They found that the activation of cone transducin by its cognate cone visual pigment was fivefold slower than the activation of rod transducin by rhodopsin. There is a contradictory result, though. *Xenopus* violet cone visual pigment expressed in COS-1 cells activated rod transducin as efficiently as rhodopsin did [30]. However, the relevance of the in vitro data to the situation in intact cells is unclear. The rates of production of rod T* by rod R* were substantially lower in these experiments, sometimes by orders of magnitude, than the benchmark value derived from physiological and biochemical data for rods [18]. Obviously, multiple factors other than possible differences between rod and cone visual pigments and transducins affect the results of in vitro measurements.

The efficiency of interaction between R* and T in rods and cones was also studied through physiological methods using a heterologous expression of cone proteins in rods. The results were contradictory and thus inconclusive. For instance, the expression of mouse green cone pigment in mouse rods reduced the amplification approximately fourfold without a major change in the response kinetics [31]. The expression of cone T_{α} in mouse rods decreased the sensitivity of photoresponse and accelerated its kinetics [32]. On the other hand, expressing the blue-sensitive (S) mouse cone visual pigment in mouse rods had no effect on the single-photon response [33]. Deng et al. [34] expressed cone T_{α} in mouse rods and rod T_{α} in mouse cones, and concluded that rod and cone transducins are functionally equivalent. Similarly, no difference between mouse rod photoresponses was observed when testing all four possible patterns of expression of rod and cone visual pigments and rod and cone T_{α} [35]. To add to the uncertainty, expression of cone PDE in mouse rods increased the

sensitivity of the photoresponse [36]. Of special interest is the experiment designed by nature. Amphibian retinas contain two types of blue-sensitive photoreceptors—so-called green rods and blue-sensitive cones that are spectrally identical. In the salamander, both have been shown to express the same short wavelength–sensitive 2 (SWS-2) cone visual pigment, but cones use cone-specific transducin, while green rods use rod transducin [37]. In this study, it appeared that blue cones needed 5 to 28 times more light falling on them than green rods to produce photoresponses of the same amplitude, while the kinetics of the response did not markedly change [37]. Kawakami and Kawamura [38] recently argued that the right way to assess the amplification in the cascade is to compare sensitivities to incident (rather than absorbed) light. We further support their conclusion (see below). Thus, the results in [37] suggest that the amplification in salamander blue cones is substantially lower than in green rods naturally expressing the same visual pigment.

Physiological experiments on photoreceptors heterologously expressing various rod- and cone-specific visual pigments and transducins have their own problems. First, genetic manipulations apparently strictly targeted to the desired protein may also have poorly traceable effects on other components of the phototransduction cascade. Second, and perhaps more importantly, these experiments mostly deal with "unnatural" combinations of visual pigments and transducins that may not be selected by evolution to work together in the same cell. Thus, whatever the results are, they do not answer the main question: What is the reason(s) for different sensitivities of rods and cones naturally expressing their own visual pigments, transducins, and other components of the phototransduction cascade?

To address this question, we compared photoresponses of frog rods and fish *Carassius* cones recorded at the time resolution sufficient to obtain undistorted activation phases. The results were interpreted within the framework of a specially designed mathematical model of phototransduction. Parameters of the model were constrained by measurements when calcium feedback was disabled by fixing cytoplasmic Ca^{2+} concentration. These constraints unambiguously allowed the biochemical amplification and characteristic times of the cascade turnoffs to be determined. We found that there was a large scatter among individual cones with respect to their amplification. However, maximum amplification observed in cones was as high as in rods. The approximately three orders of magnitude lower sensitivity of the "worst" cones compared to rods resulted from approximately tenfold lower biochemical amplification and a tenfold acceleration of all turnoff reactions (quenching of photoactivated visual pigment and phosphodiesterase, dark cGMP turnover, and calcium feedback).

METHODS

Selecting experimental animals: At first glance, it seems ideal to compare amplification in rods and cones from the same species. This, however, may not be the right approach. Different animal species have different visual tasks, and interspecies differences are reflected, for instance, in rod or cone dominance in the retina. This may not only be related to the number and size of photoreceptors, but also to their biochemical and physiologic properties. Thus, one could expect all combinations of "good" and "poor" rods and cones to exist in different retinas. For proper comparison, one needs rods and cones representing the best examples in their class. Another prerequisite is the big size and robustness of the cells that would allow easy experimental manipulations. We tested the frog retina, whose rods are among the largest and most sensitive known. It appeared that it is possible to record from frog cones, but the cells were small and fragile, making Ca^{2+}-clamping experiments unfeasible. A good source of cones could be the retina of fish, for instance, of carp or *Carassius*. Again, it appeared impossible to carry out Ca^{2+}-clamp experiments on *Carassius* rods to complement cone data, since the rods were highly fragile and unstable. Thus, we chose frog rods and fish cones for comparison. Working on frog rods and *Carassius* cones also had an important advantage in relation to any other animal, because a large body of biochemical and physiological data on these and closely related species is available. This facilitated the interpretation of our data in terms of underlying biochemical mechanisms.

Animals and preparations: Experiments were performed on rods and cones of the frog *Rana ridibunda* (*Pelophylax ridibundus*) and on cones of the fish *Carassius carassius*. Frogs were caught from the Volga River (southern Russia) and kept for up to 6 months in tanks with free access to water at 18 to 20 °C on a natural day/night cycle, and fed living cockroaches and dry pet food. Fish were obtained from a local hatchery. They were kept in aerated aquaria on a 12 h:12 h light–dark cycle and fed dry fish food. Animals were treated in accordance with the Guide for the Care and Use of Laboratory Animals (1996, National Academy of Sciences, Washington, DC) and with the rules approved by the local Institutional Animal Care and Use Committee.

Prior to the experiment, the animals were dark-adapted overnight. They were killed by decapitation and double-pithed under dim red light. Further manipulations were carried out under infrared (IR) TV control. Procedures to prepare the samples for electrophysiological recordings were described

in detail earlier [39,40]. Briefly, eyes were enucleated and retinas removed into a Ringer-filled Petri dish. Small retinal pieces were transferred to a drop of the solution on a coverslip and finely chopped with a razor blade. The resulting mixture of tiny retinal pieces and isolated photoreceptors was placed in the perfusion chamber. The photoreceptor current was recorded using the standard suction pipette recording technique [41]. Most of the data were obtained from intact rods and cones protruding from retinal pieces, in the configuration OS in. To conduct measurements at a fixed cytoplasmic Ca^{2+} concentration, isolated *Carassius* cones were held in the suction pipette *inner segment in*, and their OSs were subjected to the Ca^{2+}-clamping solution using a fast solution changer. The changer consisted of an assembly of movable tubings. A two-barrel pipette made of a theta capillary produced two jets of solutions of different composition. The second, single-barrel pipette placed opposite to the theta tubing at the distance of ≈ 0.5 mm sucked the jets in, thus preventing their mixing with the main bath solution that was always perfused with slowly flowing normal Ringer. A computer-controlled stepper motor could move the tubing assembly so that the OS was suddenly immersed into either of the two jets of different composition [39].

Solutions: The standard Ringer solution used for retinal dissection and as the main solution in the perfusion bath contained for frog the following ingredients (in mM): NaCl 90, KCl 2.5, $MgCl_2$ 1.4, glucose 10, $CaCl_2$ 1, $NaHCO_3$ 5, HEPES 5, bovine serum albumin (BSA) 50 mg/l, and EDTA 0.05, with pH adjusted to 7.6. For fish, the solution contained the following: NaCl 102, KCl 2.6, $MgCl_2$ 1, glucose 5, $CaCl_2$ 1, $NaHCO_3$ 28, HEPES 5, and BSA 50 mg/l, and the pH was adjusted to 7.8–8.0. The composition of each solution was chosen to ensure stable long-lasting recordings, high dark current and maximum sensitivity in corresponding species.

To block Ca^{2+} feedback onto the cascade, we used the Ca^{2+}-clamping solution based on the recipe in [42] for fish cones. This contained the following: guanidine-Cl 102, KCl 2.6, $KHCO_3$ 28, glucose 5, HEPES 5, and EGTA 4, with pH adjusted to 7.8–8.0 by tetramethylammonium hydroxide (TMA-OH). Free Ca^{2+} concentration in this solution was calculated to be below 1 nM. Ca^{2+}-clamping solution for frog rods was as in [39]. All chemicals were from Sigma-Aldrich (St. Louis, MO).

Light stimulation: The light stimulation system consisted of two independent channels based on high-output light-emitting diodes (LEDs), one with λ_{max} = 519 nm, and the other with λ_{max} = 632 nm. By comparing sensitivities at the two wavelengths, it was possible to discriminate spectral classes of the photoreceptors (red-sensitive versus green-sensitive versus blue-sensitive cones in the goldfish, and red rods versus green rods in the frog). Stimulus intensity was controlled by switchable neutral density (ND) filters and LED current. Standard flash duration was 2 ms. Flash intensity, expressed as the number of isomerizations per flash (R*), was calibrated for each individual frog rod using the statistics of few-photon responses [41]. Cell dimensions were determined from the IR monitor screen, the number of rhodopsin molecules per rod outer segment (ROS) calculated, and intensity was further expressed as the fractional bleach or as the number of photons per square micrometer. The latter was used to estimate the number of activated visual pigment molecules in *Carassius* cones. Independently, intensity was calibrated using a Burr-Brown OPT-310 integrated optosensor. The two calibrations coincided within 20%.

Data acquisition: Photoresponses were low-pass filtered at 300 Hz (8-pole analog Bessel filter), digitized at 2 ms intervals and stored on the computer hard disk. If necessary, further digital filtering could be applied to the data. Proper reference to the digital filtering is given in the figure legends. Data acquisition, stimulus timing, and stimulus intensity were under LabView hardware and software control (National Instruments, Austin, TX).

Microspectrophotometry: To estimate light collecting areas (F) of photoreceptors in the population of animals used in the study, we measured absorbances and OS sizes of cones and rods by microspectrophotometry. The design of the microspectrophotometer (MSP) and the measurement procedures were described in detail earlier [43,44]. Briefly, small pieces of dark-adapted isolated retinas were placed in a drop of appropriate physiological saline on a coverslip and teased apart by needles to obtain solitary photoreceptors or their outer segments. The sample was covered by another coverslip, sealed at the edges with petroleum jelly and placed on the MSP stage. Width of the measuring beam was set to 3 μm for frog rods, and 2 μm for *Carassius* cones, and its length was about 2/3 of the OS length. Recordings from the OSs were taken at two polarizations of the measuring beam (T, transversal with respect to the OS axis, and L, longitudinal, along the axis). This allowed more accurate estimation of the absorption of the nonpolarized light used for stimulation. Baylor et al.'s [41] formula for the cell light collecting area was used with a small modification:

Equation 1

$$F = \frac{\pi d^2}{4} \cdot q \cdot \ln(10) \cdot f \cdot a_{max} \cdot S(\lambda) = V_{OS} \cdot q \cdot \mathrm{n}(10) \cdot f \cdot a_{max} \cdot S(\lambda)$$

Here, d is the ROS diameter (µm), l is the ROS length (µm), and V_{OS} is the volume of a cylindrical OS. For conical OSs, $V_{OS} = \pi \cdot (d_b^2 + d_b \cdot d_t + d_t^2) \cdot l / 12$, where d_b and d_t are OS diameters at the base and tip. In addition, $q = 0.67$ is the quantum yield of the visual pigment bleaching, and a_{max} is the specific T-density at λ_{max} of the corresponding visual pigment. F is measured in µm^2. As estimated from MSP recordings, $a_{max} = 0.0151 \pm 0.0015$ µm^{-1} for A1-based frog rods, and $a_{max} = 0.012 \pm 0.0025$ µm^{-1} for A2-based *Carassius* cones (average ± standard deviation [SD] of 24 rods and 27 cones). The L/T ratio was 0.23 for rods and 0.27 for cones. $S(\lambda)$ is the relative spectral sensitivity at the wavelength of stimulation as determined from the visual pigment templates [43]. Red- and green-sensitive *Carassius* cones had $\lambda_{max} = 613$ and 539 nm, respectively. Factor $f = 0.5 \cdot (1+L/T)$ applies to the situation where OS is illuminated side-on with nonpolarized light, as in our setup.

Definition and experimental determination of biochemical amplification in the phototransduction cascade: an analysis: The generally accepted definition of biochemical amplification in phototransduction has been formulated by Pugh and Lamb [15,45,46]. As shown by the authors, if turnoff processes are neglected, the initial part of a current response $r(t)$ to a short flash of light should follow a squared parabolic time course:

Equation 2

$$r(t) / r_{max} = \frac{1}{2} \cdot A \cdot R^* \cdot (t - t_{eff})^2$$

Here, r_{max} is the maximum response that corresponds to complete closure of the CNG channels, R^* is the number of photoactivated visual pigment molecules, t_{eff} is the phototransduction delay, and A is the amplification constant (s^{-2}). A is expressed via the parameters of the phototransduction cascade:

Equation 3

$$A = \nu_{RE} \cdot \frac{k_{cat}}{K_M} \cdot n_{cG} \cdot \frac{10^{15}}{N_{Av} \cdot V_{cyto}}$$

Here, ν_{RE} (s^{-1}) is the rate of production of T*/PDE* by a single R^*, k_{cat} is the maximum hydrolytic activity of a PDE* subunit (s^{-1}), K_M is the PDE Michaelis constant (here in mol/l), and n_{cG} is the Hill's coefficient of the CNG channel gating by cGMP. Avogadro's number, $N_{Av} = 6 \cdot 10^{23}$ mol^{-1}, and the cytoplasmic volume of the OS, V_{cyto} (µm^3), convert number of molecules to concentration. Factor 10^{15} converts liters to µm^3. The cytoplasmic volume of the OS (V_{cyto}) is assumed to be 1/2 V_{OS} [15,46].

The A-value can apparently be extracted from a simple parabolic fit to an initial part of the normalized photoresponse. The analysis does not involve any complicated treatment and relies on a simple theory. This is why the amplification constant has gained general acceptance as a tool for characterizing signal amplification in photoreceptors. The definition has its problems, though. The first problem arises from the fact that the amplification constant A depends not only on molecular parameters of the cascade, such as ν_{RE}, k_{cat}, K_M, and n_{cG}, but also on the OS volume V_{cyto} (Equation (3)). Obviously, the same biochemical machinery initiated by the absorption of a single photon would produce a greater effect in smaller cells [46]. Thus, the comparison of photoreceptors of different size (e.g., rods versus cones) based on the A-value is meaningless. A higher amplification constant does not necessarily mean that underlying biochemistry works faster, or vice versa.

This problem can be solved by expressing stimulus strength as the intensity of the incident light $I(\lambda)$ rather than as the number of photoactivated rhodopsins R^*. R^* in Equation (2) can be calculated as:

Equation 4

$$R^* = I(\lambda) \cdot F = 2 \cdot V_{cyto} \cdot I(\lambda) \cdot q \cdot \ln(10) \cdot f \cdot a_{max} \cdot S(\lambda)$$

Here, $I(\lambda)$ is measured in photons·µm^{-2}, and $2 \cdot V_{cyto}$ stands for V_{OS} in Equation (1). Inserting this into Equation (2) and taking into account Equation (3), one obtains:

Equation 5

$$r(t) / r_{max} = I(\lambda) \cdot q \cdot \ln(10) \cdot f \cdot a_{max} \cdot S(\lambda) \cdot \nu_{RE} \cdot \frac{k_{cat}}{K_M} \cdot n_{cG} \cdot \frac{10^{15}}{N_{Av}} (t - t_{eff})^2$$

Thus, V_{cyto} vanishes from the equation. Let us now define effective light intensity $I_e(\lambda)$ (photoisomerizations·µm^{-3}) as:

Equation 6

$$I_e(\lambda) = I(\lambda) \cdot q \cdot \ln(10) \cdot f \cdot a_{max} \cdot S(\lambda)$$

Its meaning is the number of photoactivated visual pigment molecules *per unit volume* of the OS. To maintain similarity with Equation (2), Equation (5) can be rewritten as:

Equation 7

$$r(t) / r_{max} = I_e(\lambda) \cdot A_m \cdot \frac{10^{15}}{N_{Av}} (t - t_{eff})^2$$

Here, the modified amplification constant A_m only includes biochemical parameters of the phototransduction cascade and does not depend on the cell's volume:

Equation 8

$$A_m = v_{RE} \cdot \frac{k_{cat}}{K_M} \cdot n_{cG}$$

An additional advantage of this definition is that the effective light intensity does not depend on the cell size. Rather, it is expressed via a directly measurable physical quantity, that is, the surface density of photon flux *I(λ)*. In other words, cells with the same A_m value—rods or cones, irrespective of their size—have to exhibit the same rising phase of the response at the same irradiance level.

Recently, Kawakami and Kawamura [38] suggested a slightly different way of eliminating the cell volume from the definition of amplification, by expressing stimulus intensity as fractional bleach. Our modified amplification constant A_m is equivalent to their index of the gain *G*. If A_m is expressed in $s^{-2} \cdot \mu M^{-1}$, it can be converted to G ($fL \cdot s^{-2}$) by:

Equation 9

$$G = \frac{A_m}{N_{Av}} \cdot 10^{21}$$

The second, at a first glance technical, problem is how to extract the amplification in either sense from experimental recordings. As clearly stated in [46], the parabolic approximation of the initial phase of the photoresponse *is only valid if all recovery processes can be neglected*. These processes include the following: R* quenching by phosphorylation, T* quenching by GTP hydrolysis, prestimulus steady cGMP turnover, and active restoration of the cGMP level by Ca^{2+} feedback via GC. Parameters of these turnoffs are mostly unknown, so it is hard to tell what stretch of the initial phase of the response can be used to determine *A*. Roughly 10% of the time to the peak of the flash response seems a reasonable guess. This means that in amphibian rods, the proper stretch is about 100 ms, but it may not be longer than 10 to 15 ms in mammalian rods or in the cones of cold-blooded animals. For mammalian cones, the stretch appropriate for fitting does not exceed a few milliseconds. In addition, routinely used 10–20 ms stimuli cannot be considered as flashes for cones; rather, they are steps of light, which invalidates simple analysis based on second-order parabola fit. Third-order parabola fitting of the step responses, as recently introduced [47], partly ameliorates the situation, but the problem of neglected turnoff processes remains.

Unless the recordings are made in voltage-clamp mode, the response waveform is affected by an electrical low-pass filtering by the capacitance and resistance of the cell membrane. For rods, the effect is probably negligible, since the electrical time constant of amphibian rods—which is under 20 ms [15,48,49]—is substantially shorter than the time stretch available for analysis. In cones, however, the high area of the folded membrane of the OS may significantly increase the cell capacitance, hence the time constant. The typical electrical time constant of cones lies between 20 and 80 ms [49-52], thereby spoiling the entire part of the curve appropriate for fitting. An adverse effect may also arise from excessive low-pass analog filtering during recordings, and from digital filtering applied during data analysis.

It seems that only a realistic mathematical model of cone phototransduction that explicitly takes into account all of the turnoff processes and electrical filtering could allow us to quantitatively characterize all the processes that set the speed and sensitivity of the cone photoresponse. The model should be applied to a set of experimental data obtained with short (≤1–2 ms) flashes and at a good time resolution. Thus, our goal was to collect such a dataset and to develop an appropriate mathematical model to analyze it.

The general approach to mathematical modeling: To process and interpret data, we used a mathematical model of phototransduction common for rods and cones [53,54]. In this section, we focus solely on the features of the model that make it suitable for the specific goal of the work, that is, for extracting key parameters of the cone and rod phototransduction cascade with a minimum of ambiguity and arbitrary assumptions. The model includes all basic mechanisms that participate in the cascade activation and quenching, and Ca^{2+}-feedback regulations imposed on it. However, to make the model less redundant and more manageable, we use a phenomenological description of each process, omitting mechanistic details that are important but unnecessary here. For instance, activation of transducin by R* is a multistage process whose detailed description includes five reactions and depends on over 10 (essentially unknown) rate constants [55,56]. For our purpose, it can be convolved into a linear activation with a certain rate v_{RE} (s^{-1}) and possible delay t_{eff} [15,45,46]. The task of the modeling is to extract the two parameters' values from the experimental data. Similarly, the turnoff of light-activated visual pigment depends on its multiple phosphorylation. Yet the resulting time course of the decay of R* catalytic activity derived from a detailed model by Hamer et al. [55] could satisfactorily be approximated with a single exponential. Only the time constant of the exponential is necessary for our model.

On the other hand, the description of certain steps in many existing models is oversimplified. For instance, cGMP hydrolysis by PDE and Ca^{2+} pumping by the exchanger are often treated as linear reactions, neglecting their

Michaelis-like kinetics. Turnoff processes are commonly neglected when trying to extract the rate of the activation of the cascade from experimental recordings and so on. The price of these oversimplifications cannot be estimated a priori without more detailed experimental and model analysis. Thus, we constructed a minimum essential model (MEM) based on maximally realistic phenomenological descriptions of each key reaction without involving unnecessary mechanistic details. The complete set of equations comprising the model is given in Appendix 1.

The MEM, however minimal, contains over 30 parameters. Some of their values are (relatively) reliably known from direct measurements (e.g., k_{cat} and K_M of the PDE, or the parameters of the control of the GC by Ca^{2+} and of the CNG channel gating by cGMP; for the sources of the data, see Appendix 1). Some others are mainly interdependent scaling factors that can be relatively freely varied when fitting the model to experimental data. However, many parameters are crucial for the model functioning, but their values are just guessed and can differ by orders of magnitude among the models available in literature. The resulting freedom of fitting makes quantitative conclusions derived from modeling mostly meaningless. Therefore, we conducted a special set of measurements using Ca^{2+}-clamp protocol. It provided a wealth of information on the dark and light-dependent cGMP turnover. This allowed strong experimental constraints to be imposed on many crucial parameters of the model. Corresponding experiments and procedures of analysis are described in detail in Appendix 1. All computations were performed using MathCad 2001i (MathSoft, Cambridge, MA).

RESULTS

Basic features of rod and cone photoresponses: Figure 1 shows a series of photoresponses to flashes of varying intensities recorded from a frog rod (A) and two *Carassius* cones (B, C). The shapes of the rod and cone responses are basically similar, save the fact that cone responses are an order of magnitude faster and approximately three orders of magnitude less sensitive. However, there is a cone-specific feature of the response that is already incipient in Figure 1B, and fully expressed in Figure 1C. In B, the slope of the front of the response saturates at modest intensities, and further increase of the intensity mostly shortens the delay of the front without making it steeper. An extreme example of this behavior is seen in Figure 1C, where all responses follow the same initial trajectory, peeling away at progressively later times with increasing intensities. This feature was not specific for green-sensitive cones (as shown in Figure 1C). Saturation of the slope of the front was to various extents evident in all spectral types of cones, including a few recorded blue-sensitive cells. Responses of this sort were earlier recorded from cones of fish (*Carassius*, *Danio* [57,58]) and salamander [50,52,59]. The response versus intensity function for all types of cones was satisfactorily described by a Michaelis-like relation:

Equation 10

$$r / r_{\max} = \frac{I}{I + I_{05}}$$

where $I_{0.5}$ is the flash intensity at which the response amplitude is half-maximum (Figure 2). Rod response versus

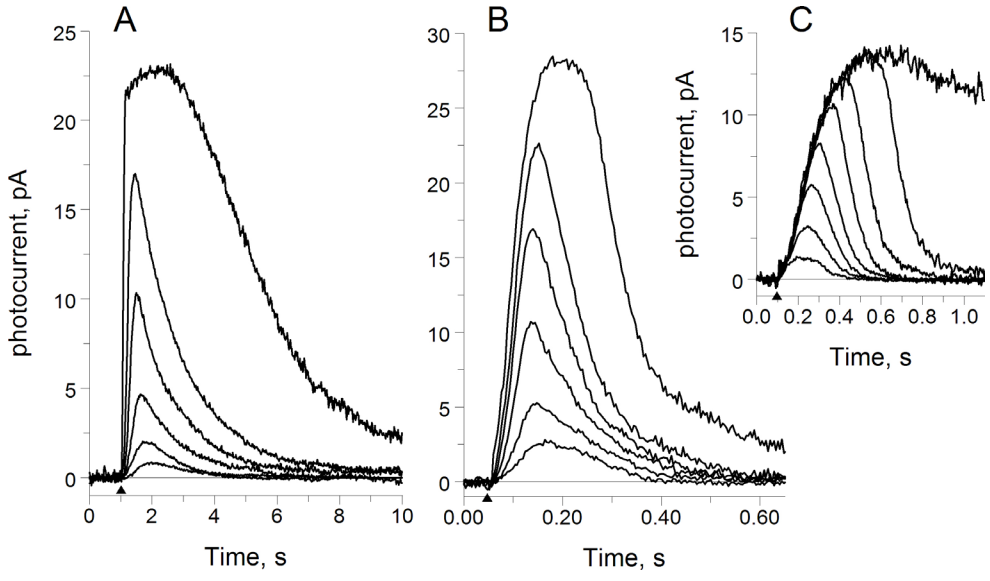

Figure 1. Comparison of photoresponses of rods and cones to a series of flashes of various intensities. Flash duration: 2 ms, wavelength: 519 nm. Upward triangles mark the moment of the flash. **A**: Frog red rod. Intensities: 0.19, 0.48, 1.2, 4.2, 10.6, and 260 photons·μm^{-2} per flash. **B**: Red-sensitive *Carassius* cone. Intensities: 865, 2,170, 5,450, 13,700, 34,400, and 300,000 photons·μm^{-2} per flash. **C**: Green-sensitive *Carassius* cone. Intensities: 1,370, 3,440, 8,650, 21,700, 75,300, 189,000, 475,000, and 2,370,000 photons·μm^{-2} per flash.

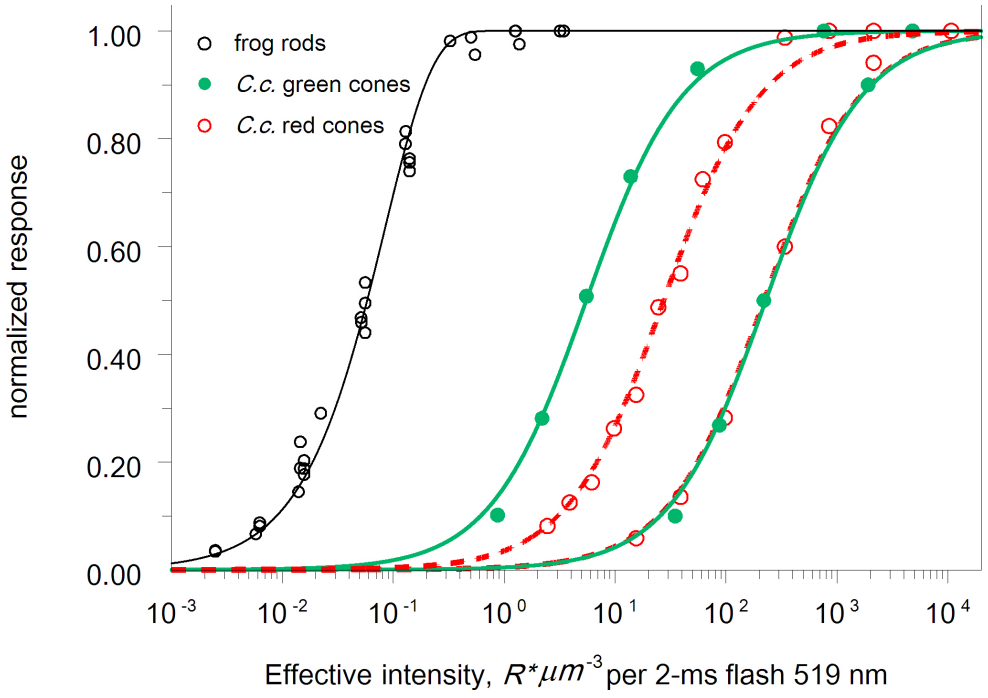

Figure 2. Response versus intensity curves for frog rods and *Carassius* cones. Black circles: rods; red and green circles: cones. Green solid curves through filled circles mark the most- and least-sensitive green cones. Red curves through empty circles show the range of scatter of red cone data. Curves were drawn by the least-squares method using Equation (10) for cones, and (10a) for rods. Graphs are plotted versus effective light intensity I_e as defined in Equation (6).

intensity dependence was steeper and better described by an exponential saturation function:

Equation 10a

$$r / r_{\max} = 1 - \exp(-I / I_{0.63})$$

On average, green cones were more light-sensitive than red ones. However, the scatter of sensitivity among individual cells even of the same spectral type was quite large, exceeding an order of magnitude in green cones. Sensitivity did not obviously correlate with the speed of the photoresponse. The scatter of the time to peak (T_{peak}) and the response integration time (T_i) was modest, at about 25% (SD/mean). There was no statistically significant difference in these parameters among red and green cones (Table 1).

Mathematical modeling: The series of responses like those in Figure 1B,C clearly show a saturation of the speed of the PDE activation even at modest-intensity stimuli. Thus, the full series cannot be fitted with our model, where the PDE activity is scaled linearly with intensity. Therefore, we only used for fitting the responses to the weakest flashes whose fractional amplitude did not exceed 20%.

Throughout the modeling, many parameters, mostly characterizing the steady state in the dark, were fixed at the values taken from literature (Appendix 1, Table A2). Subject to change during fitting were the parameters that determine the sensitivity and the time course of the photoresponse. These are the rate of transducin/PDE activation by photo-activated visual pigment (v_{RE}), the rates of R* and PDE* quenching (k_R and k_E), and basal (dark) cGMP turnover rate

Table 1. Basic characteristics (time to peak, integration time, and sensitivity) of rod and cone flash responses whose amplitudes lie within the linear range (fractional response *R/RMAX* ≤0.2).

Parameters	t_{peak}, ms ± SEM	Integration time, ms ±SEM	$I_{0.5}$, R*·μm^{-3} per flash ± SEM
Green-sensitive cones (13)	108±7	165±8	49±16 *
Red-sensitive cones (12)	101±8	143±12	81±18 *
Rods (5)	680±80	1560±145	0.063±0.002

* Difference between green- and red-sensitive cones is statistically significant at p<0.05 (Mann–Whitney test).

α_{dark}/cG_{dark}. Crucial factors are also the kinetics and amplification of the Ca^{2+} feedback loop. With the exception of v_{RE}, all of the parameters were initially assigned the guess values obtained from the Ca^{2+}-clamp experiments (Appendix 1, Table A3). After that, adjusting v_{RE} usually allowed a model flash response approaching the experimental one to be obtained. Further v_{RE}, k_R, k_E, α_{dark}, τ_e, and parameters of the Ca^{2+} buffer were finely tuned for best fit. Tuning was carried out by trial and error, and the quality of the fit was judged from the coefficient of the correlation between the model and the experimental response. Necessary adjustments of k_R, k_E, α_{dark}, τ_e, and *FB* were usually within ± 15% of the initial values, although approximately one-fifth of cones needed larger deviations from the average. The rate of T*/PDE* production v_{RE}, however, varied greatly, in line with a big scatter of sensitivity among individual cones (Figure 2). Figure 3 shows sample fits of the photoresponses of the cone with maximum amplification (A), the cone with minimum amplification (B), and a "typical" rod (C).

Values of the parameters specific for individual cells from Figure 3 are given in Table 2. Average data on the rates of activation and inactivation of the phototransduction cascade in rods and cones are summarized in Table 3. It is obvious that there is a big scatter in the amplification parameters among individual cones. Noticeably, in the most sensitive green cones, the rate of activation of the cGMP hydrolysis (which determines the biochemical amplification) is virtually equal to that in rods. However, both deactivation reactions (R* and PDE* quenching), dark cGMP turnover, and Ca^{2+} feedback in all cones were about 10 times faster.

DISCUSSION

Uniqueness of the fits and validity of cascade parameters estimated from the Ca^{2+} clamp: We found that cone photoresponses could be successfully fitted by our model using values of the parameters partially taken from literature and partially constrained by or derived from our measurements with the Ca^{2+} clamp. The question arises of whether the fits are unique, and the answer is that they are definitely not. Fits were highly sensitive to change of any single key parameter like v_{RE}, a_{dark}, k_R, k_E, or K_{ex}. However, wildly different parameters of the cascade turnoff might yield equally good fits to the experimental data as soon as compensatory changes to other components are allowed. For instance, the effect of fivefold slowing of the dark turnover rate (α_{dark}/cG_{dark}) and 330-fold reduction of K_{ex} in the model can be compensated by appropriate acceleration of k_R and k_E and adjustments of the parameters of the Ca^{2+} buffer (Figure 3B, Table 4). This sensitivity of the model fits to even small changes of a single parameter and the possibility to compensate it by proper changes in others has been observed previously [32,52]. However, the experimental constraints on the set of parameters that we obtained with the Ca^{2+} clamp allowed us to reduce the ambiguity of the fits and derive robust estimates of biochemical values from the model.

Biochemical amplification: cones versus rods: It would be tempting to calculate the rate of activation of the cascade, v_{RE}, directly from the *PDE*(t)* derived from the Ca^{2+}-clamp experiments. This would avoid any ambiguity inherent to multiparametric model fits. Unfortunately, this is precluded by the high noise level of the Ca^{2+}-clamp data on cones (see Appendix 1, Figure A3, A5). Reducing the noise by averaging multiple responses is not feasible because the Ca^{2+}-clamp procedure deteriorates the cell. Averaging across many cones makes no sense due to the large scatter of the amplification among individual cells (Table 3).

Fortunately, it appears that the uncertainty of the values of the shape-forming parameters ($\alpha_{dark}/cGMP_{dark}$, k_R, k_E, and Ca^{2+} buffering, constrained by the Ca^{2+} clamp) had only a weak effect on the estimate of v_{RE}, which determines the speed of the activation of the cascade (hence, amplification). As long as the set of the shape parameters provided a good fit of the model to the experimental response, variation of v_{RE} did not exceed a few percent. However, membrane filtering had a stronger effect on the estimate of amplification. Amplification and τ_e were to a certain extent interchangeable, so an approximate 10% change of amplification can be compensated by an adjustment of τ_e and possibly other parameters without markedly reducing the quality of the fit. However, further reduction of v_{RE} below the optimum value distinctly deteriorated fit statistics. Thus, we believe that the uncertainty of our values of amplification is within about 15%.

We found that the biochemical amplification, as defined in this work, can vary by about an order of magnitude among individual cones. In addition, the red-sensitive cones are on average less sensitive than green-sensitive cells (Figure 1, Table 1), and this is mostly due to their lower amplification (Table 3). We made no attempt to identify the morphological types of the cones we recorded from (large or small single cones, members of double cones, etc.). However, differences in properties of individual cone types may be the cause of the observed variability. This idea is in line with large variability of cones' absolute sensitivity found earlier on the striped bass retina [60]. The variability was clearly related to the morphological and spectral type of the cell, red-sensitive "fast" twins being 40 times less sensitive than green-sensitive singles.

Variation in sensitivity and amplification among frog red rods was far less prominent (Figure 2; Table 3). The "best"

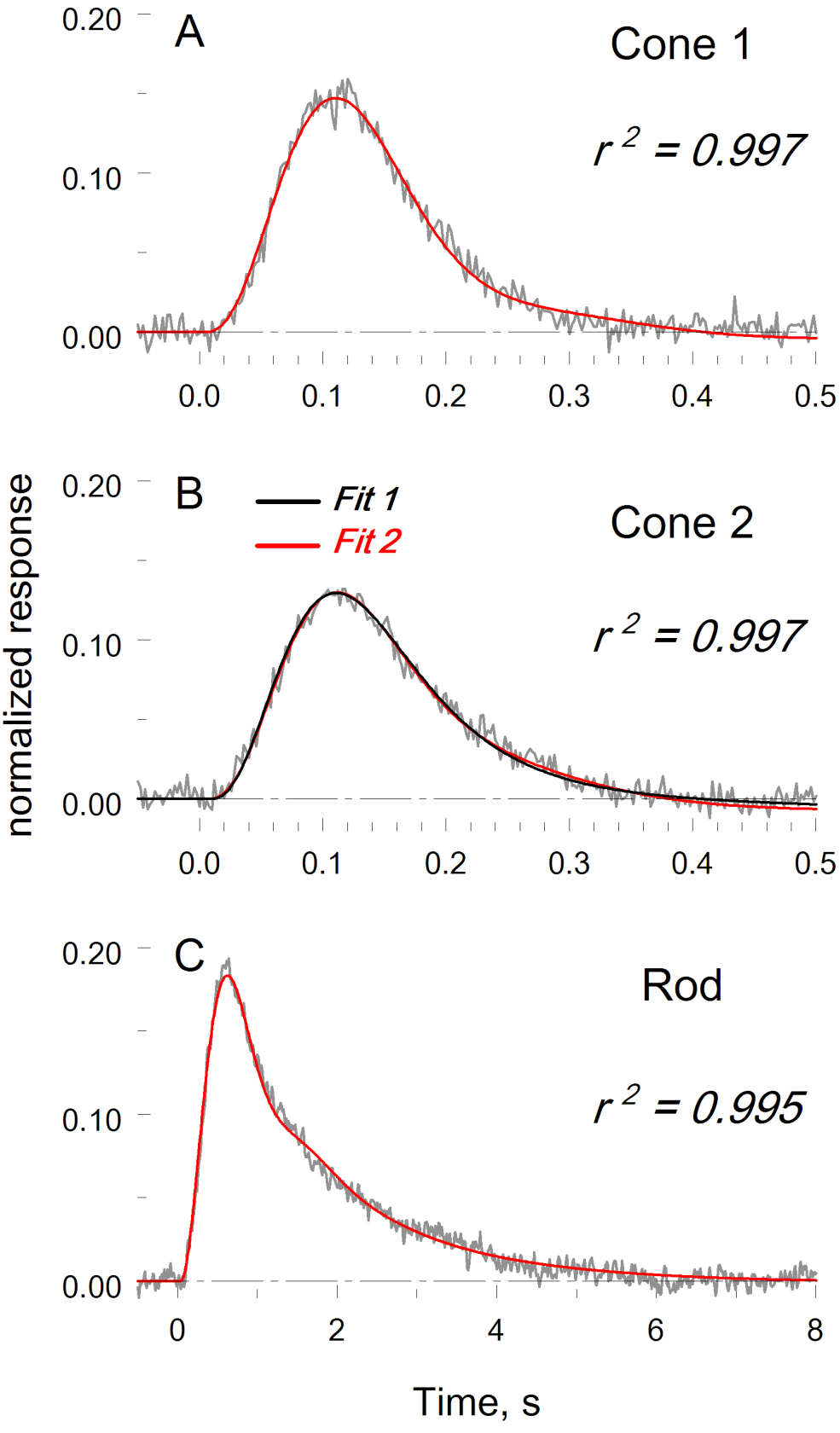

Figure 3. Sample model fits to cone and rod flash responses. Flash: 2 ms, 519 nm. **A**: *Carassius* "green" cone, which exhibited maximum amplification. Average of 40 responses; effective intensity: 2.1 $R^*{\cdot}\mu M^{-3}$. **B**: The *Carassius* "red" cone with the lowest amplification. Average of 24 responses; effective intensity: 25 $R^*{\cdot}\mu M^{-3}$. Two alternative fits with drastically different parameters are shown to illustrate the ambiguity of an unrestrained model. Parameters of the fits are given in Table 4. **C**: Frog rod. Average of 10 responses; effective intensity: 0.028 $R^*{\cdot}\mu M^{-3}$. Noisy lines: nonfiltered experimental responses; smooth lines: model fits with the parameters given in Table 2. The coefficient of correlation between the experimental and model curves in **A**–**C** is between 0.995 and 0.997.

Table 2. Biochemical parameters of a rod and two cones as derived from model fitting. Same cells as in Figure 3. Definition of the parameters is given in Appendix 1.

Parameter	Units	Cone 1	Cone 2	Rod
j_{dark}	pA	11.5	12.5	20.2
α_{dark}/cG_{dark}	s^{-1}	13.4	11.6	1.15
k_{Rdark}	s^{-1}	12.9	13.1	1.5
$k_{E,}$ s^{-1}	s^{-1}	13.5	13	1.4
v_{RE}	s^{-1}	430	30	220
t_{eff}	ms	4	2.5	27
a_P	-	0.025	0.05	0.09
k_{Arr}	s^{-1}	3	3.5	1
FB	-	31	27	35
B_{max}	µM	240	230	270
k_1	μM^{-1} s^{-1}	2	2	1
k_{-1}	s^{-1}	1	1	0.1
τ_e	ms	27	31	17
A_m	$s^{-2}\cdot\mu M^{-1}$	$11.8\cdot10^4$	$0.85\cdot10^4$	$12.1\cdot10^4$

Table 3. Average parameters of activation and quenching of rods and cones.

Parameters	Green-sensitive cones (7)	Red-sensitive cones (9)	Rods (5)
v_{RE}, s^{-1}	228±56 * range: 62 - 430	93±17 * range: 30 - 200	200±14 range: 180 - 220
A_m, $s^{-2}\cdot\mu M^{-1}$	$(6.3\pm1.5)\cdot10^4$ * range: (1.7 – 11.8)·10^4	$(2.6\pm0.48)\cdot10^4$ * range: (0.85 – 5.5)·10^4	$(11\pm0.8)\cdot10^4$ range: (9.9 – 12.1)·10^4
k_{Rdark}, s^{-1}	11.3±0.8	12.7±2.6	1.4±0.07
k_E, s^{-1}	12.4±1.1	10.6±1.7	1.2±0.14
α_{dark}/cG_{dark}, s^{-1}	11.2±1	11.9±0.7	0.96±0.14
$Ca^{2+}{}_{fast}$, ms	51	51	408

Data are given as Mean ± SEM *Difference between green- and red-sensitive cones is statistically significant at p<0.05 (Mann–Whitney test). $Ca^{2+}{}_{fast}$ is the time constant of the faster, major component of light-induced Ca^{2+} decline (Figure 5A). Other parameters are defined in Appendix 1, Table A1.

Table 4. Ambiguity of fitting the response with a poorly restrained model. Key kinetics and sensitivity parameters of two fits to cone response in Figure 3B are given.

Parameter	Units	Fit 1	Fit 2
cG_{dark}	µM	6	3
α_{dark}/cG_{dark}	s^{-1}	11.6	2.17
k_{Rdark}	s^{-1}	13.1	23.6
k_E	s^{-1}	13	25
v_{RE}	s^{-1}	30	38.5
K_{ex}	µM	1.66	0.005
FB	-	27	10

cells yielded A_m = 12.1·10^4 s^{-2}·µM^{-1}, which corresponded to v_{RE} = 220 s^{-1}, k_{cat} = 2200 s^{-1}, and K_M = 10 µM, that is, close to the benchmark values established for amphibian rods in a specially designed biochemical and electrophysiological study [18]. Remarkably, the cones with maximum amplification yielded virtually the same result, as follows: A_m = 11.8·10^4 s^{-2}·µM^{-1} which stemmed from v_{RE} = 430 s^{-1}, k_{cat} = 2,200 s^{-1}, and K_M = 20 µM (Table 2, cone 1). It should be noted that the amplification is an integrated parameter that depends on v_{RE}, the rate of activation of PDE by R*, and on PDE* catalytic properties k_{cat} and K_M (Equation (8)). The three properties are completely interchangeable, and only A_m could unambiguously be determined from modeling. The exact values of cone k_{cat} and K_M are not quite certain [19,21,23], so for instance, if one assumes cone k_{cat} = 2,200 s^{-1} and K_M = 10 µM, like in rods, the resulting v_{RE} = 215 s^{-1} also becomes identical to that in rods.

Our A_m values can be compared with equivalent G-values obtained in [38] on carp rods and red-sensitive cones, as well as bullfrog rods. The authors found that the gain in frog and carp rods is approximately four times higher than in red-sensitive carp cones. This is similar to the 4.2:1 ratio found by us for A_ms of frog rod and average *Carassius* red cone (Table 3). In addition, amplification in best *Carassius* green-sensitive cones was four times higher than the *Carassius* average red cone, which makes them similar to bullfrog and carp rods. However, if converted to G, our absolute values of amplification are about two times higher than those found by Kawakami and Kawamura [38] in the carp and bullfrog. This apparent discrepancy can be explained by the fact that the authors determined amplification by routine parabolic fitting, which neglects turnoff processes. As we further show, neglecting turnoffs leads to an approximately 1.6-fold underestimation of amplification. Taking into account the scatter of experimental data, our results are in fair agreement with the results in [38].

Equal amplification values of the "best" green-sensitive cones and frog rods (Table 3) suggest that the R*-T-PDE interaction in cones may proceed as fast as in rods. A wide scatter of the amplification among individual cones can plausibly be explained by varying levels of expression of transducin, among other possibilities. It is also obvious that biochemical samples, in which many cones are pooled, should on average exhibit a lower rate of PDE activation than rods or the "best" cones. This may explain the biochemical results from Kawamura's group [10,27-29] that consistently found two- to fivefold lower rate of T*/PDE* production in carp cone preparations compared to rods.

Reactions of the cascade turnoff in cones: The reactions that control the restoration of the dark state work in a concerted way. Therefore, the three main parameters, $\alpha_{dark}/cGMP_{dark}$, k_R, and k_E, are also interchangeable to a great extent and cannot unambiguously be found solely from model fitting without additional experimental constraints. Fortunately, Ca^{2+}-clamp data provided the constraints; it appeared that the three rates are close to each other and are an order of magnitude faster than in rods (Table 3).

The dark cGMP turnover rate: The rate of the turnover of the cytoplasmic cGMP pool is an important factor that contributes to the control of the speed of the photoresponse and to light adaptation [61]. The dark turnover rate T_r (s^{-1}) can be found as:

Equation 11

$$T_r = \frac{a_{dark}}{cG_{dark}}$$

Here, the rate of cGMP synthesis (dark activity of GC) α_{dark} is expressed in µM·s^{-1} and the concentration of cGMP is expressed in µM. Since the cone responses are approximately 10-fold faster than rod responses (Figure 1), it could be expected that the activity of GC in cones is correspondingly higher. This is indeed the case, as shown by biochemical measurements on carp cones [62].

Equation (11) is a bit deceptive, though, since it gives the impression that the dark turnover rate is proportional to the activity of GC, and conceals the fact that α_{dark} affects cG_{dark} as well. From the equation of cGMP turnover:

Equation 12

$$\frac{dcG(t)}{dt} = \alpha(t) - \beta(t) \cdot \frac{cG(t)}{cG(t) + K_M}$$

one can find:

Equation 13

$$T_r = \frac{\beta_{dark}}{cG_{dark} + K_M}$$

At $cG_{dark} << K_M$, that is, at low α_{dark}, this yields:

Equation 14

$$T_r = \frac{\beta_{dark}}{K_M}$$

This means that the turnover rate is set by the catalytic activity of phosphodiesterase rather than GC, which is lacking from Equation (14). Excess activation of synthesis

(hence an increase of cG_{dark}) actually *decreases* T_r (Equation (13)). This suggests that the primary cause of the accelerated cGMP turnover in cones is high dark PDE activity.

Our estimate of T_r in *Carassius* cones based on Ca^{2+}-clamp measurements and supported by model fitting is about 10 s^{-1}; values below 5 s^{-1} can decidedly be rejected (see Appendix 1, Figure A5A). This is in agreement with more direct measurements with the isobutylmethylxanthine (IBMX)-jump on salamander cones. In these cells, whose flash response is two to three times slower than in *Carassius* cones, $T_r \approx 2$ to 3 s^{-1} [63-65]. As for the increased activity of GC in cones found in [62], it may be a compensatory effect caused by the need to keep a proper dark cGMP concentration.

Quenching the photoactivated cascade: The flash-evoked wave of the PDE* activity is shaped by quenching of R* and active T_α-GTP/PDE complexes at the rates of k_R and k_E, respectively. At a fixed $[Ca^{2+}]_{in}$, each reaction can be approximated by an exponential, which finally yields a two-exponential *PDE*(t)* curve:

Equation 15

$$PDE^*(t) = A \cdot (\exp(-t/\tau_2) - \exp(-t/\tau_2))$$

Here, A is a scaling factor that is proportional to stimulus intensity and amplification, and τ_1 and τ_2 are the time constants of the two turnoff reactions. If $k_R > k_E$, $\tau_1 = 1/k_E$ and $\tau_2 = 1/k_R$; otherwise, τ_1 and τ_2 are swapped. We determined k_R and k_E in Ca^{2+}-clamp experiments (Appendix 1, Figure A5B). Similarly to the dark cGMP turnover, they appeared approximately 10 times faster than in rods (Table 2, Table 3).

Figure 4 supports the validity of the turnoff parameters estimated this way. Panel A shows a model fit of a cone flash response in normal Ringer. Fitting was initiated from crude average estimates of $\alpha_{dark}/cGMP_{dark}$, k_R, and k_E, found as explained in Appendix 1, Figures A3, A5, A6, Table A3 and refined by small adjustments of the three parameters, v_{RE}, and Ca^{2+}-buffering. The wave of PDE activity was then derived from the model (smooth red line in panel B). The light-induced PDE activity was also found from the response of the same cell in Ca^{2+}-clamp condition using the model-derived $\alpha_{dark}/cGMP_{dark}$ value (gray noisy curve in B). The black line in B represents a two-exponential least square fit to the gray (Ca^{2+}-clamp) curve. It is seen that the $\beta_1(t)$ time courses obtained experimentally from the Ca^{2+}-clamped response and from model fitting are in fair agreement.

Both reactions of the quenching of the photoactivated cascade, at R* and at the T* stage, proceed in cones roughly 10 times faster than in rods (Table 3). It has been shown that the active conformation of a visual pigment, meta II, decays in cones almost 100 times faster than in rods [66-68]. Still, the characteristic time of decay of meta II of *Carassius* red- and green-sensitive cones is about 5 s, which is 50-fold slower than necessary for timely turnoff of transducin activation. Obviously, the fast quenching of cone R* is ensured by

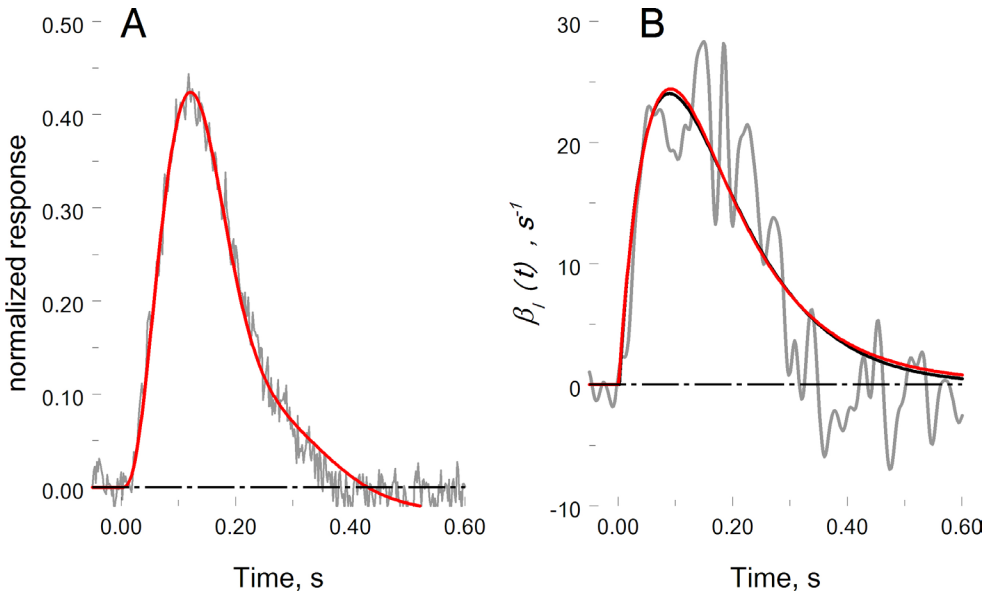

Figure 4. Testing the validity of the cascade turnoff parameters derived from Ca^{2+}-clamped responses, as described in Appendix 1. **A**: A cone flash response (noisy curve) fitted with the model whose key parameters were roughly restrained by average Ca^{2+}-clamp data (smooth curve). **B**: The red line shows light-induced PDE activity $\beta_1(t)$ derived from the model in A. The gray noisy line is $\beta_1(t)$ derived from Ca^{2+}-clamped response of the same cone to an identical flash. The curve is Gauss-filtered with a 20 ms window. A smooth black line shows the least-square fit to the gray curve with Equation (15), where A=634 s^{-1}, τ_1=0.093 s, and τ_2=0.084 s. The fit is in a fair agreement with the model-derived curve.

phosphorylation via cone-specific rhodopsin-kinase (GRK7), whose level of expression and specific activity are substantially higher than those of GRK1 in rods [69-73].

As for the rate of T*/PDE* turnoff, it is controlled in rods by the level of expression of the GTPase activating complex RGS9/Gβ5 [74-78]. It seems that this is true of cones as well, since the level of RGS9/Gβ5 in cones is much higher than that in rods [20,28,79].

The two rates of quenching, k_R and k_E, are close to each other (Table 2) and are basically interchangeable in the model. Therefore, neither of the two can unambiguously be assigned to R* or PDE* quenching. Recently, it was found [42,80] that the so-called dominant time constant of the cascade turnoff in salamander cones is Ca-dependent. This points to Ca^{2+}-recoverin-dependent R* quenching as the slower process. However, in rods, PDE* quenching may also be adaptation-(supposedly Ca^{2+}-) dependent [59,81,82]. Besides, our analysis suggests that k_R and k_E are almost identical, which calls into question the notion of the dominant turnoff process, at least in *Carassius* cones.

Calcium turnover: Ca^{2+} feedback is decisive in shaping the dark-adapted photoresponse and supporting light adaptation [59,83-87]. Thus, the speed of cytoplasmic Ca^{2+} changes is one of the crucial factors for proper model (and cone) functioning. In our model, the time course of $[Ca^{2+}]_{in}$ is set by a balance between Ca^{2+} influx via the CNG channels, its extrusion by the Ca, K/Na exchanger, and interaction with two sort of intracellular buffers [53,88]. One of the buffers equilibrates with $[Ca^{2+}]_{in}$ quickly and can be characterized by its buffering power *FB* [89]. The second buffer, of a larger capacity, operates slowly and is mostly responsible for shaping the tail of the flash response (Appendix 1 equations (A11), (A12)). Correspondingly, after instant closure of the CNG channels, the intracellular free Ca^{2+} concentration ($[Ca^{2+}]_{in}$) declines along an approximately two-exponential curve. As derived from the modeling, the fast phase has an average time constant of 51 ms and an amplitude of about 70% of the total $[Ca^{2+}]_i$ decline. The slow phase has a time constant of 1.6 s and an amplitude of about 30% of the total $[Ca^{2+}]_i$ decline (Figure 5A, Table 3). Ca^{2+}-sensitive dye measurements also show a two-exponential $[Ca^{2+}]_{in}$ decline of similar parameters, at least in regard to the major fast phase. Its time constant is about 140 ms in salamander cones [90], about 160 ms in visible light-sensitive cones of zebrafish [91], and 255 ms in zebrafish ultraviolet (UV)-sensitive cones [92]. Taking into account that the *Carassius* cone responses are two to three times faster than in salamander and zebrafish, our model-derived values for the fast phase are in good agreement with the results of direct measurements. As for the slow phase, it is hard to tell how the model data for low-intensity responses may be related to the slow phase of $[Ca^{2+}]_{in}$ decline seen in fluorescent measurements mostly performed with high-intensity stimuli [90-92]. The slow phase in bright light conditions may result from Ca^{2+} release from a different sort of high-capacity binding site.

In rods, modeled Ca^{2+} decline also exhibited two-exponential kinetics. The fast phase had an average time constant of 408 ms and an amplitude of about 66% of the total $[Ca^{2+}]_i$ decline (Table 3). The slow phase had a time constant of 9.6 s and an amplitude of about 34% of the total $[Ca^{2+}]_i$ decline. Thus, the major component of the Ca^{2+}-feedback signal in cones was approximately eight times faster than in rods.

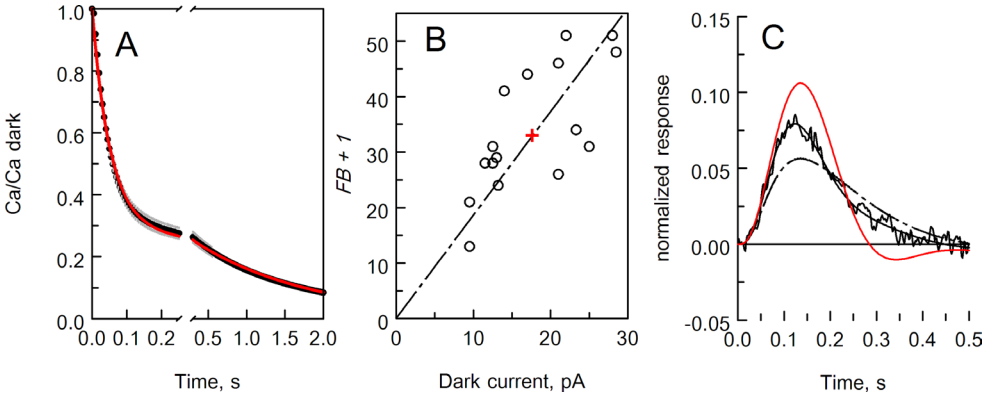

Figure 5. Parameters of Ca^{2+} turnover in cones derived from the model. **A**: Average time course of the decay of free Ca^{2+} concentration after instantaneous closure of the CNG channels. Mean of 16 cells ± standard error of the mean (SEM). The red line is a two-exponential approximation of average data, with relative amplitudes of 0.694 and 0.306, and time constants of 51 ms and 1.57 s, respectively. **B**: Correlation of the buffering power of the fast Ca^{2+} buffer (*FB*) with the cone's dark current. Circles mark individual cells. The straight line is a least-square linear fit to data forced to pass through zero. The red cross marks an (imaginary) cone whose dark current and *FB* value correspond to the average of the population. **C**: Effect of *FB* value on the shape of the model response. The solid smooth line over the noisy curve shows the best-fitting model, *FB* = 43. Dot-dashed line: model response with *FB* = 11; smooth red line: model response with *FB* = 86.

There is a technical problem with determining Ca^{2+} buffering parameters from modeling. The rate of the cytoplasmic Ca^{2+} turnover is set by the ratio of ionic influx through the CNG channels to the OS cytoplasmic volume V_{cyto} and to *FB*. In most models, including ours, V_{cyto} is fixed at a certain average value. However, modeled cells may differ widely in respect to the dark current, and hence in respect to the Ca^{2+} influx, which is a fixed fraction of the current. Therefore, the *FB* value should be scaled proportionally to the dark current if the kinetics of $[Ca^{2+}]_{in}$ changes is to be preserved. Figure 5B shows that indeed there is an approximately linear relationship between cone experimental j_{dark} and *FB* derived from the model. This suggests that the Ca-buffering properties are approximately constant among the cells. The cross in Figure 5B marks the "average" cone with an average dark current of 17.6 pA and average *FB* = 33 ± 3 (standard error of the mean [SEM]). If it also corresponds to the average V_{cyto} = 0.06 pl assumed in the model, the amount of Ca^{2+} bound to it in darkness is 16.5 ± 1.5 µmol per liter of the cytoplasmic volume.

As for the slow buffer, its binding capacity B_{max} shows no clear correlation with j_{dark} (not shown). The average value of B_{max} in the model is approximately 280 µM.

The time course and magnitude of light-induced Ca^{2+} changes depend on the properties of the Na^+/Ca^{2+}-K^+ exchanger. The exchanger is characterized by its maximum activity j_{exsat} and Michaelis' constant K_{ex}. As soon as K_{ex}, dark Ca^{2+} concentration and f_{Ca}, the fraction of channel current carried by Ca^{2+}, are fixed—as in our model—j_{exsat} should be chosen to counterbalance Ca^{2+} influx at a given j_{dark}:

Equation 16

$$j_{exsat} = f_{Ca} \cdot j_{dark} \cdot (1 + K_{ex} / [Ca]_{dark}) / 2$$

If $K_{ex} >> [Ca^{2+}]_{dark}$, the exchanger operates in a linear mode. This means that after a sudden closure of a fraction of the CNG channels, $[Ca^{2+}]_i$ decreases exponentially to a new steady level that is proportional to the fraction of the current left. Notably, the magnitude of the $[Ca^{2+}]_i$ decline *does not depend on* f_{Ca}. On the other hand, if $K_{ex} << [Ca^{2+}]_{dark}$, the exchanger operates mostly at its maximum speed. Then, in the light, $[Ca^{2+}]_i$ decreases at a constant rate until it reaches a level close to or below $K_{ex} << [Ca^{2+}]_{dark}$, where the speed of the extrusion becomes dependent on $[Ca^{2+}]_{in}$. Only then can a new balance between inward and outward fluxes be achieved. This behavior does not depend either on the fraction of the channels closed or on f_{Ca}, so even a small steady decrease of j_{dark} would result in a drastic reduction of $[Ca^{2+}]_{in}$.

The linear or nearly linear mode of operation of the exchanger ($[Ca^{2+}]_{dark}/K_{ex}$ <1) is assumed in most available models, including ours. This is strongly supported by the results in [84] and [93]. Here, the authors showed that loading rods or cones with a saturating Ca^{2+} concentration results in an exchanger current that is several fold larger than the current seen in dark-adapted, non-loaded cells. In line with this are approximately exponential (rather than linear) light-induced $[Ca^{2+}]_{in}$ declines, measured experimentally by fluorescent dyes [90-92]. During steady background illumination, the Ca^{2+} concentration falls in proportion to the dark current blocked [92], which also points to an approximately linear mode of the exchanger operation.

A strongly nonlinear regime is postulated by Korenbrot [51], who assumes $[Ca^{2+}]_{dark} / K_{ex}$ ratio from 16 to 80. This assumption contradicts the experimental data on Ca^{2+} kinetics (above). In addition, as shown in Appendix 1 (Equation (A24)), Michaelis-like nonlinearity at the stages of cGMP hydrolysis and Ca^{2+} extrusion affects the loop gain of the Ca^{2+} feedback. Our measurements of the gain set the limit of $(1 + cGMP_{dark} / K_M) \cdot (1 + [Ca^{2+}]_{dark} / K_{ex}) \leq 1.7$. This excludes a situation where $K_{ex} < [Ca^{2+}]_{dark}$.

The speed of the Ca^{2+} feedback is crucial for properly shaping the photoresponse. The feedback signal should match the time courses of other turnoff processes like R* and PDE* quenching. Feedback that is too rapid (where the *FB* value is too low) makes the response slower rather than faster, and reduces sensitivity (dot-dash curve in Figure 5C). Feedback that is too slow (where the *FB* value is too high) makes the response oscillatory (Figure 5C, solid red curve). This suggests that Ca^{2+} changes in cones should be roughly tenfold faster than in rods, proportionally to the speed of their photoresponse. As our modeling shows, this is indeed the case.

Interestingly, drastically different parameters of Ca^{2+} turnover in rods and cones may stem from a single simple factor, the OS volume. The turnover rate is set by the ratio of the Ca^{2+} influx to the volume of the OS cytoplasm. Thus, a smaller size of cone OS *at approximately the same dark current* inevitably makes the feedback in cones faster than in rods. The difference in the OS membrane topology, and hence the big difference in surface-to-volume ratio between cone and rod OSs, is as such irrelevant to setting the speed of the Ca^{2+} feedback. This has already been noticed [48,84]. A higher area of the OS membrane in cones may be secondary to the task of maintaining proper dark current through a smaller OS.

The price of oversimplification: Whatever the definition of the amplification is, its value can be found from a parabolic

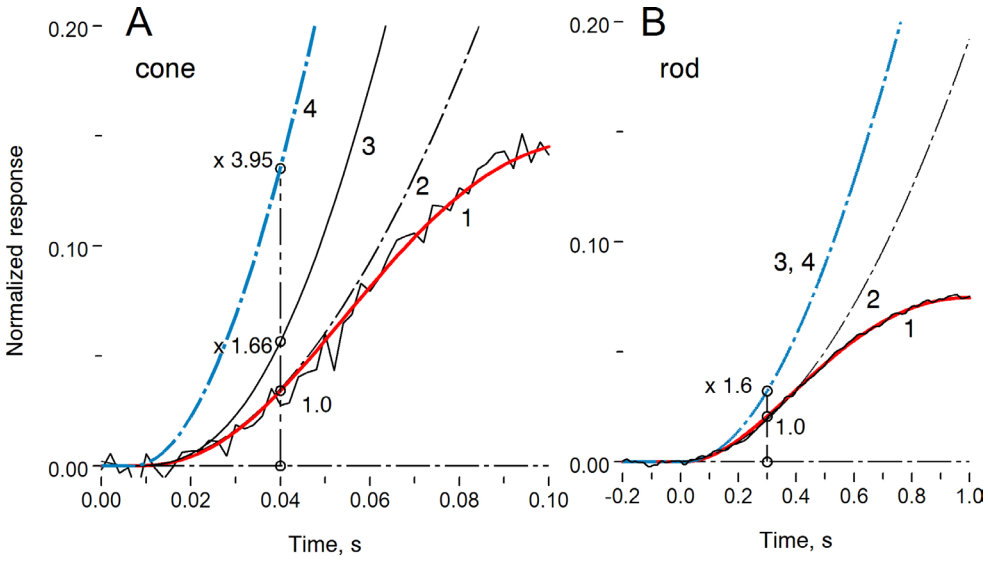

Figure 6. Errors of determining the amplification constant introduced by simplified parabolic fitting of the initial part of the response. The experimental responses are normalized in a routine way, that is, to the dark current, which consists of the CNG channel current plus the exchanger current. **A**: *Carassius* cone. Noisy curve: experimental response of a cone to 2 ms flash applied at time zero; red line 1: the model best fitted to the entire response; line 2: least-square fit to the initial 40 ms part of the response with the routinely used Pugh and Lamb [15,45,46] parabola (Equation (2)); line 3: the response of the model in which all turnoff processes and Ca^{2+} feedback are disabled, and the model response is normalized to the dark CNG-channel current alone (excluding the exchanger current); line 4: same as line 3, but in addition, the cell time constant is set to zero. Curve 4 represents the "real" parabola behind the experimental response; it yields an amplification value that is four times higher than would be derived from routine fitting (curve 2). **B**: Same as A, but for a frog rod. Curves 3 and 4 coincide because the effect of membrane filtering in rods is negligible. Routine parabolic fitting results in a 1.6-fold underestimate of amplification.

fitting of the initial part of the experimental flash response (Equation (2)) *if all complicating factors (turnoff reactions, membrane filtering, and technical problems) can be neglected*. The question is, what is the price of the oversimplification in real life?

Figure 6A shows an initial phase of a cone response (noisy curve) with the best-fitting model curve superimposed on it (smooth line 1). Dot-dashed line 2 is a parabolic fit (Equation (2)) to the 0–40 ms stretch of the experimental response; it accurately fits the model response as well. However, the definition of A (in either sense) deals with the responses normalized to the light-suppressible current j_{cGdark}. Thus, it should exclude the exchanger current which is $1/2 \cdot f_{Ca} j_{cGdark}$. If $f_{Ca} = 0.2$, as we assumed, then an 11% correction has to be applied. Further, the model allows disabling of the calcium feedback and recovery reactions (dark cGMP turnover, R* and PDE* turnoffs). The model then generates the response shown by the curve 3. Its steepness is 66% higher than the steepness of parabolic fit 2. If the filtering by the cell's electrical time constant (22 ms in this cell) is also eliminated, the resulting model response follows dot-dashed curve 4. Line 4 is the response that would be generated by a cell that meets prerequisite for the applicability of Pugh and Lamb [15,45,46] analysis (no turnoffs, no feedback, no low-pass filtering, normalized to the dark cGMP-gated current). Fitting it with the parabola would yield the "real" amplification value, which is exactly equal to $v_{RE} \cdot (k_{cat}/K_M) \cdot n_{cG}$ derived from the model. It appears four times higher than derived from the parabolic fitting to the raw response (curve 1). Thus, the routine parabolic fitting results in a fourfold underestimate of the biochemical amplification in *Carassius* cones. The error must be even higher in mammalian cones, whose photoresponses are substantially briefer than those of fish cones [94-98]. In amphibian rods, the error introduced by routine analysis is approximately 1.6-fold (Figure 6B).

Why are cones less sensitive than rods?: What is the contribution of individual factors to lower sensitivity of cones compared to rods? We suggested a new definition of biochemical amplification in phototransduction that is independent of the cell's size and only includes molecular parameters of the cascade. These are the rate of PDE activation by R^* (v_{RE}), the catalytic activity of PDE* (k_{cat}/K_M), and cooperativity of channel gating n_{cG} (Equation (8); see also [38]). Only their product A_m could be determined from physiological experiments, and it appeared that in the most sensitive cones, the amplification can be as high as in rods (Table 3). This suggests that there is nothing inherently different between the processes of activation of the cone and rod phototransduction. Hence, the main factor that reduces sensitivity of cones is their faster turnoff. This can be illustrated by a simple example.

The red-sensitive cone 2 shown in Figure 3B is 2,260 times less sensitive than the rod in the same figure, panel C. (Sensitivities are compared using effective light intensities, to eliminate differences in light capture between rhodopsin rods and porphyropsin cones.) Its amplification, though, is just 14 times lower. The remaining 160-fold sensitivity reduction is due to an approximately 10-fold acceleration of all turnoff reactions, as well as electrical filtering (Table 2). The leading role of the speed of turnoff reactions in setting cones' sensitivity has already been suggested based on biochemical data [10,27,28,38]. Keeping amplification high and accelerating the response termination appears to be a wise evolutionary strategy. It exchanges sensitivity for the speed of the reaction in the most efficient way.

APPENDIX 1.

To access the data, click or select the words "Appendix 1."

ACKNOWLEDGMENTS

The authors declare no conflict of interest. This work was supported by grant 1B-05 from the Biologic Branch of the Russian Academy of Sciences and grant 13–04–00701a from the Russian Foundation for Basic Research to VG. Preliminary results were presented at the 12th International Conference on Vision (Visionarium-XII, Tvärminne, Finland, 2013). The authors are thankful to Ian Dick for his help with English text, and to anonymous Molecular Vision reviewers whose comments improved the manuscript.

REFERENCES

1. Sacks O. The island of the colorblind. A.A. Knopf (NY): Distributed by Random House; 1997.
2. Arshavsky VY, Lamb TD, Pugh EN Jr. G proteins and phototransduction. Annu Rev Physiol 2002; 64:153-87. [PMID: 11826267].
3. Arshavsky VY, Burns ME. Photoreceptor signaling: supporting vision across a wide range of light intensities. J Biol Chem 2012; 287:1620-6. [PMID: 22074925].
4. Arshavsky VY, Burns ME. Current understanding of signal amplification in phototransduction. Cell Logist 2014; 4:e29390-[PMID: 25279249].
5. Burns ME, Baylor DA. Activation, deactivation, and adaptation in vertebrate photoreceptor cells. Annu Rev Neurosci 2001; 24:779-805. [PMID: 11520918].
6. Burns ME, Arshavsky VY. Beyond counting photons: trials and trends in vertebrate visual transduction. Neuron 2005; 48:387-401. [PMID: 16269358].
7. Chen CK. The vertebrate phototransduction cascade: amplification and termination mechanisms. Rev Physiol Biochem Pharmacol 2005; 154:101-21. [PMID: 16634148].
8. Fain GL, Matthews HR, Cornwall MC, Koutalos Y. Adaptation in vertebrate photoreceptors. Physiol Rev 2001; 81:117-51. [PMID: 11152756].
9. Fain GL, Hardie R, Laughlin SB. Phototransduction and the evolution of photoreceptors. Curr Biol 2010; 20:R114-24. [PMID: 20144772].
10. Kawamura S, Tachibanaki S. Rod and cone photoreceptors: molecular basis of the difference in their physiology. Comp Biochem Physiol A Mol Integr Physiol 2008; 150:369-77. [PMID: 18514002].
11. Lamb TD, Pugh EN Jr. Phototransduction, dark adaptation, and rhodopsin regeneration the Proctor lecture. Invest Ophthalmol Vis Sci 2006; 47:5137-52. [PMID: 17122096].
12. Luo DG, Xue T, Yau KW. How vision begins: an odyssey. Proc Natl Acad Sci USA 2008; 105:9855-62. [PMID: 18632568].
13. Palczewski K. G protein-coupled receptor rhodopsin. Annu Rev Biochem 2006; 75:743-67. [PMID: 16756510].
14. Palczewski K. Chemistry and biology of vision. J Biol Chem 2012; 287:1612-9. [PMID: 22074921].
15. Pugh EN Jr, Lamb TD. Phototransduction in vertebrate rods and cones: molecular mechanisms of amplification, recovery and light adaptation. In: Stavenga DG, Pugh EN Jr., de Grip WJ, editors. Handbook of Biological Physics. New York: Elsevier Science; 2000. p. 183–255.
16. Wensel TG. Signal transducing membrane complexes of photoreceptor outer segments. Vision Res 2008; 48:2052-61. [PMID: 18456304].
17. Yau KW, Hardie RC. Phototransduction motifs and variations. Cell 2009; 139:246-64. [PMID: 19837030].
18. Leskov IB, Klenchin VA, Handy JW, Whitlock GG, Govardovskii VI, Bownds MD, Lamb TD, Pugh EN Jr, Arshavsky VY. The gain of rod phototransduction: reconciliation of biochemical and electrophysiological measurements. Neuron 2000; 27:525-37. [PMID: 11055435].
19. Gillespie PG, Beavo JA. Characterization of a bovine cone photoreceptor phosphodiesterase purified by cyclic GMP-sepharose chromatography. J Biol Chem 1988; 263:8133-41. [PMID: 2836413].
20. Zhang X, Wensel TG, Kraft TW. GTPase regulators and photoresponses in cones of the eastern chipmunk. J Neurosci 2003; 23:1287-97. [PMID: 12598617].
21. Muradov H, Boyd KK, Haeri M, Kerov V, Knox BE, Artemyev NO. Characterization of human cone phosphodiesterase-6 ectopically expressed in *Xenopus laevis* rods. J Biol Chem 2009; 284:32662-9. [PMID: 19801642].
22. Muradov H, Boyd KK, Artemyev NO. Rod phosphodiesterase-6 PDE6A and PDE6B subunits are enzymatically equivalent. J Biol Chem 2010; 285:39828-34. [PMID: 20940301].

23. Huang D, Hinds TR, Martinez SE, Doneanu C, Beavo JA. Molecular determinants of cGMP binding to chicken cone photoreceptor phosphodiesterase. J Biol Chem 2004; 279:48143-51. [PMID: 15331594].

24. Imai H, Kojima D, Oura T, Tachibanaki S, Terakita A, Shichida Y. Single amino acid residue as a functional determinant of rod and cone visual pigments. Proc Natl Acad Sci USA 1997; 94:2322-6. [PMID: 9122193].

25. Kojima K, Imamoto Y, Maeda R, Yamashita T, Shichida Y. Rod visual pigment optimizes active state to achieve efficient G protein activation as compared with cone visual pigments. J Biol Chem 2014; 289:5061-73. [PMID: 24375403].

26. Vissers PM, Bovee-Geurts PH, Portier MD, Klaassen CH, DeGrip WJ. Large-scale production and purification of the human green cone pigment: characterization of late photo-intermediates. Biochem J 1998; 330:1201-8. [PMID: 9494086].

27. Tachibanaki S, Tsushima S, Kawamura S. Low amplification and fast visual pigment phosphorylation as mechanisms characterizing cone photoresponses. Proc Natl Acad Sci USA 2001; 98:14044-9. [PMID: 11707584].

28. Tachibanaki S, Yonetsu S, Fukaya S, Koshitani Y, Kawamura S. Low activation and fast inactivation of transducin in carp cones. J Biol Chem 2012; 287:41186-94. [PMID: 23045532].

29. Koshitani Y, Tachibanaki S, Kawamura S. Quantitative aspects of cGMP phosphodiesterase activation in carp rods and cones. J Biol Chem 2014; 289:2651-7. [PMID: 24344136].

30. Starace DM, Knox BE. Activation of transducin by a *Xenopus* short wavelength visual pigment. J Biol Chem 1997; 272:1095-100. [PMID: 8995408].

31. Sakurai K, Onishi A, Imai H, Chisaka O, Ueda Y, Usukura J, Nakatani K, Shichida Y. Physiological properties of rod photoreceptor cells in green-sensitive cone pigment knock-in mice. J Gen Physiol 2007; 130:21-40. [PMID: 17591985].

32. Chen J, Woodruff ML, Wang T, Concepcion FA, Tranchina D, Fain GL. Channel modulation and the mechanism of light adaptation in mouse rods. J Neurosci 2010; 30:16232-40. [PMID: 21123569].

33. Shi G, Yau KW, Chen J, Kefalov VJ. Signaling properties of a short-wave cone visual pigment and its role in phototransduction. J Neurosci 2007; 27:10084-93. [PMID: 17881515].

34. Deng WT, Sakurai K, Liu J, Dinculescu A, Li J, Pang J, Min SH, Chiodo VA, Boye SL, Chang B, Kefalov VJ, Hauswirth WW. Functional interchangeability of rod and cone transducin alpha-subunits. Proc Natl Acad Sci USA 2009; 106:17681-6. [PMID: 19815523].

35. Mao W, Miyagishima KJ, Yao Y, Soreghan B, Sampath AP, Chen J. Functional comparison of rod and cone Gα(t) on the regulation of light sensitivity. J Biol Chem 2013; 288:5257-67. [PMID: 23288843].

36. Deng WT, Sakurai K, Kolandaivelu S, Kolesnikov AV, Dinculescu A, Li J, Zhu P, Liu X, Pang J, Chiodo VA, Boye SL, Chang B, Ramamurthy V, Kefalov VJ, Hauswirth WW. Cone phosphodiesterase-6α' restores rod function and confers distinct physiological properties in the rod phosphodiesterase-6β-deficient rd10 mouse. J Neurosci 2013; 33:11745-53. [PMID: 23864662].

37. Ma J, Znoiko S, Othersen KL, Ryan JC, Das J, Isayama T, Kono M, Oprian DD, Corson DW, Cornwall MC, Cameron DA, Harosi FI, Makino CL, Crouch RK. A visual pigment expressed in both rod and cone photoreceptors. Neuron 2001; 32:451-61. [PMID: 11709156].

38. Kawakami N, Kawamura S. Difference in the gain in the phototransduction cascade between rods and cones in carp. J Neurosci 2014; 34:14682-6. [PMID: 25355220].

39. Astakhova LA, Firsov ML, Govardovskii VI. Kinetics of turn-offs of frog rod phototransduction cascade. J Gen Physiol 2008; 132:587-604. [PMID: 18955597].

40. Astakhova LA, Samoiliuk EV, Govardovskii VI, Firsov ML. cAMP controls rod photoreceptor sensitivity via multiple targets in the phototransduction cascade. J Gen Physiol 2012; 140:421-33. [PMID: 23008435].

41. Baylor DA, Lamb TD, Yau KW. Responses of retinal rods to single photons. J Physiol 1979; 288:613-34. [PMID: 112243].

42. Zang J, Matthews HR. Origin and control of the dominant time constant of salamander cone photoreceptors. J Gen Physiol 2012; 140:219-33. [PMID: 22802362].

43. Govardovskii VI, Fyhrquist N, Reuter T, Kuzmin DG, Donner K. In search of the visual pigment template. Vis Neurosci 2000; 17:509-28. [PMID: 11016572].

44. Kolesnikov AV, Golobokova EY, Govardovskii VI. The identity of metarhodopsin III. Vis Neurosci 2003; 20:249-65. [PMID: 14570247].

45. Lamb TD, Pugh EN Jr. A quantitative account of the activation steps involved in phototransduction in amphibian photoreceptors. J Physiol 1992; 449:719-58. [PMID: 1326052].

46. Pugh EN Jr, Lamb TD. Amplification and kinetics of the activation steps in phototransduction. Biochim Biophys Acta 1993; 1141:111-49. [PMID: 8382952].

47. Mahroo OA, Ban VS, Bussmann BM, Copley HC, Hammond CJ, Lamb TD. Modeling the initial phase of the human rod photoreceptor response to the onset of steady illumination. Doc Ophthalmol 2012; 124:125-31. [PMID: 22350929].

48. Cobbs WH, Pugh EN Jr. Kinetics and components of the flash photocurrent of isolated retinal rods of the larval salamander, *Ambystoma tigrinum*. J Physiol 1987; 394:529-72. [PMID: 2832596].

49. Makino CL, Taylor WR, Baylor DA. Rapid charge movements and photosensitivity of visual pigments in salamander rods and cones. J Physiol 1991; 442:761-80. [PMID: 1818565].

50. Perry RJ, McNaughton PA. Response properties of cones from the retina of the tiger salamander. J Physiol 1991; 433:561-87. [PMID: 1841958].

51. Korenbrot JI. Speed, sensitivity, and stability of the light response in rod and cone photoreceptors: facts and models. Prog Retin Eye Res 2012; 31:442-66. [PMID: 22658984].

52. Soo FS, Detwiler PB, Rieke F. Light adaptation in salamander L-cone photoreceptors. J Neurosci 2008; 28:1331-42. [PMID: 18256253].

53. Kuzmin DG. Mathematical modeling of phototransduction and light adaptation in frog retinal rods. Sens Syst 2004; 18:305-16. Russ..

54. Kolesnikov AV, Rikimaru L, Hennig AK, Lukasiewicz PD, Fliesler SJ, Govardovskii VI, Kefalov VJ, Kisselev OG. G-protein betagamma-complex is crucial for efficient signal amplification in vision. J Neurosci 2011; 31:8067-77. [PMID: 21632928].

55. Hamer RD, Nicholas SC, Tranchina D, Lamb TD, Jarvinen JL. Toward a unified model of vertebrate rod phototransduction. Vis Neurosci 2005; 22:417-36. [PMID: 16212700].

56. Dell'Orco D, Schmidt H, Mariani S, Fanelli F. Network-level analysis of light adaptation in rod cells under normal and altered conditions. Mol Biosyst 2009; 5:1232-46. [PMID: 19756313].

57. Palacios AG, Goldsmith TH, Bernard GD. Sensitivity of cones from a cyprinid fish (*Danio aequipinnatus*) to ultraviolet and visible light. Vis Neurosci 1996; 13:411-21. [PMID: 8782369].

58. Palacios AG, Varela FJ, Srivastava R, Goldsmith TH. Spectral sensitivity of cones in the goldfish, *Carassius auratus*. Vision Res 1998; 38:2135-46. [PMID: 9797974].

59. Matthews HR, Fain GL, Murphy RL, Lamb TD. Light adaptation in cone photoreceptors of the salamander: a role for cytoplasmic calcium. J Physiol 1990; 420:447-69. [PMID: 2109062].

60. Miller JL, Korenbrot JI. Phototransduction and adaptation in rods, single cones, and twin cones of the striped bass retina: a comparative study. Vis Neurosci 1993; 10:653-67. [PMID: 8338802].

61. Nikonov S, Lamb TD, Pugh EN Jr. The role of steady phosphodiesterase activity in the kinetics and sensitivity of the light-adapted salamander rod photoresponse. J Gen Physiol 2000; 116:795-824. [PMID: 11099349].

62. Takemoto N, Tachibanaki S, Kawamura S. High cGMP synthetic activity in carp cones. Proc Natl Acad Sci USA 2009; 106:11788-93. [PMID: 19556550].

63. Cornwall MC, Matthews HR, Crouch RK, Fain GL. Bleached pigment activates transduction in salamander cones. J Gen Physiol 1995; 106:543-57. [PMID: 8786347].

64. Corson DW, Kefalov VJ, Cornwall MC, Crouch RK. Effect of 11-cis 13-demethylretinal on phototransduction in bleach-adapted rod and cone photoreceptors. J Gen Physiol 2000; 116:283-97. [PMID: 10919871].

65. Estevez ME, Kolesnikov AV, Ala-Laurila P, Crouch RK, Govardovskii VI, Cornwall MC. The 9-methyl group of retinal is essential for rapid Meta II decay and phototransduction quenching in red cones. J Gen Physiol 2009; 134:137-50. [PMID: 19635855].

66. Golobokova EY, Govardovskii VI. Late stages of visual pigment photolysis in situ: cones vs. rods. Vision Res 2006; 46:2287-97. [PMID: 16473387].

67. Ala-Laurila P, Kolesnikov AV, Crouch RK, Tsina E, Shukolyukov SA, Govardovskii VI, Koutalos Y, Wiggert B, Estevez ME, Cornwall MC. Visual cycle: Dependence of retinol production and removal on photoproduct decay and cell morphology. J Gen Physiol 2006; 128:153-69. [PMID: 16847097].

68. Estevez ME, Ala-Laurila P, Crouch RK, Cornwall MC. Turning cones off: the role of the 9-methyl group of retinal in red cones. J Gen Physiol 2006; 128:671-85. [PMID: 17101818].

69. Tachibanaki S, Arinobu D, Shimauchi-Matsukawa Y, Tsushima S, Kawamura S. Highly effective phosphorylation by G protein-coupled receptor kinase 7 of light-activated visual pigment in cones. Proc Natl Acad Sci USA 2005; 102:9329-34. [PMID: 15958532].

70. Wada Y, Sugiyama J, Okano T, Fukada Y. GRK1 and GRK7: unique cellular distribution and widely different activities of opsin phosphorylation in the zebrafish rods and cones. J Neurochem 2006; 98:824-37. [PMID: 16787417].

71. Arinobu D, Tachibanaki S, Kawamura S. Larger inhibition of visual pigment kinase in cones than in rods. J Neurochem 2010; 115:259-68. [PMID: 20649847].

72. Rinner O, Makhankov YV, Biehlmaier O, Neuhauss SC. Knockdown of cone-specific kinase GRK7 in larval zebrafish leads to impaired cone response recovery and delayed dark adaptation. Neuron 2005; 47:231-42. [PMID: 16039565].

73. Vogalis F, Shiraki T, Kojima D, Wada Y, Nishiwaki Y, Jarvinen JL, Sugiyama J, Kawakami K, Masai I, Kawamura S, Fukada Y, Lamb TD. Ectopic expression of cone-specific G-protein-coupled receptor kinase GRK7 in zebrafish rods leads to lower photosensitivity and altered responses. J Physiol 2011; 589:2321-48. [PMID: 21486791].

74. Krispel CM, Chen D, Melling N, Chen YJ, Martemyanov KA, Quillinan N, Arshavsky VY, Wensel TG, Chen CK, Burns ME. RGS expression rate-limits recovery of rod photoresponses. Neuron 2006; 51:409-16. [PMID: 16908407].

75. Pugh EN Jr. RGS expression level precisely regulates the duration of rod photoresponses. Neuron 2006; 51:391-3. [PMID: 16908403].

76. Burns ME, Pugh EN Jr. RGS9 concentration matters in rod phototransduction. Biophys J 2009; 97:1538-47. [PMID: 19751658].

77. Burns ME, Pugh EN Jr. Lessons from photoreceptors: turning off G-protein signaling in living cells. Physiology (Bethesda) 2010; 25:72-84. [PMID: 20430952].

78. Arshavsky VY, Wensel TG. Timing is everything: GTPase regulation in phototransduction. Invest Ophthalmol Vis Sci 2013; 54:7725-33. [PMID: 24265205].

79. Cowan CW, Fariss RN, Sokal I, Palczewski K, Wensel TG. High expression levels in cones of RGS9, the predominant GTPase accelerating protein of rods. Proc Natl Acad Sci USA 1998; 95:5351-6. [PMID: 9560279].

80. Matthews HR, Sampath AP. Photopigment quenching is Ca^{2+} dependent and controls response duration in salamander L-cone photoreceptors. J Gen Physiol 2010; 135:355-66. [PMID: 20231373].

81. Krispel CM, Chen CK, Simon MI, Burns ME. Novel form of adaptation in mouse retinal rods speeds recovery of phototransduction. J Gen Physiol 2003; 122:703-12. [PMID: 14610022].

82. Woodruff ML, Janisch KM, Peshenko IV, Dizhoor AM, Tsang SH, Fain GL. Modulation of phosphodiesterase6 turnoff during background illumination in mouse rod photoreceptors. J Neurosci 2008; 28:2064-74. [PMID: 18305241].

83. Nakatani K, Yau KW. Calcium and light adaptation in retinal rods and cones. Nature 1988; 334:69-71. [PMID: 3386743].

84. Nakatani K, Yau KW. Sodium-dependent calcium extrusion and sensitivity regulation in retinal cones of the salamander. J Physiol 1989; 409:525-48. [PMID: 2479741].

85. Fain GL, Lamb TD, Matthews HR, Murphy RL. Cytoplasmic calcium as the messenger for light adaptation in salamander rods. J Physiol 1989; 416:215-43. [PMID: 2607449].

86. Burns ME, Mendez A, Chen J, Baylor DA. Dynamics of cyclic GMP synthesis in retinal rods. Neuron 2002; 36:81-91. [PMID: 12367508].

87. Gross OP, Pugh EN Jr, Burns ME. Calcium feedback to cGMP synthesis strongly attenuates single-photon responses driven by long rhodopsin lifetimes. Neuron 2012; 76:370-82. [PMID: 23083739].

88. Govardovskii VI, Kuzmin DG. Light-induced Ca^{2+} release and kinetics of calcium feedback in retinal rods. Sens Syst 1999; 13:206-15. .

89. Lagnado L, Cervetto L, McNaughton PA. Calcium homeostasis in the outer segments of retinal rods from the tiger salamander. J Physiol 1992; 455:111-42. [PMID: 1282928].

90. Sampath AP, Matthews HR, Cornwall MC, Bandarchi J, Fain GL. Light-dependent changes in outer segment free-Ca^{2+} concentration in salamander cone photoreceptors. J Gen Physiol 1999; 113:267-77. [PMID: 9925824].

91. Cilluffo MC, Matthews HR, Brockerhoff SE, Fain GL. Light-induced Ca^{2+} release in the visible cones of the zebrafish. Vis Neurosci 2004; 21:599-609. [PMID: 15579223].

92. Leung YT, Fain GL, Matthews HR. Simultaneous measurement of current and calcium in the ultraviolet-sensitive cones of zebrafish. J Physiol 2007; 579:15-27. [PMID: 17124271].

93. Lagnado L, McNaughton PA. Net charge transport during sodium-dependent calcium extrusion in isolated salamander rod outer segments. J Gen Physiol 1991; 98:479-95. [PMID: 1722238].

94. Schnapf JL, Nunn BJ, Meister M, Baylor DA. Visual transduction in cones of the monkey *Macaca fascicularis*. J Physiol 1990; 427:681-713. [PMID: 2100987].

95. Smith NP, Lamb TD. The a-wave of the human electroretinogram recorded with a minimally invasive technique. Vision Res 1997; 37:2943-52. [PMID: 9425511].

96. Schneeweis DM, Schnapf JL. The photovoltage of macaque cone photoreceptors: adaptation, noise, and kinetics. J Neurosci 1999; 19:1203-16. [PMID: 9952398].

97. van Hateren JH, Lamb TD. The photocurrent response of human cones is fast and monophasic. BMC Neurosci 2006; 7:34-[PMID: 16626487].

98. Nikonov SS, Kholodenko R, Lem J, Pugh EN Jr. Physiological features of the S- and M-cone photoreceptors of wild-type mice from single-cell recordings. J Gen Physiol 2006; 127:359-74. [PMID: 16567464].

Articles are provided courtesy of Emory University and the Zhongshan Ophthalmic Center, Sun Yat-sen University, P.R. China. The print version of this article was created on 7 March 2015. This reflects all typographical corrections and errata to the article through that date. Details of any changes may be found in the online version of the article.